PNAS RESEARCH ARTICLE | BIOPHYSICS AND COMPUTATIONAL BIOLOGY
CHEMISTRY

Exploring RNA destabilization mechanisms in biomolecular condensates through atomistic simulations

Matteo Boccalini[a], Yelyzaveta Berezovska[a], Giovanni Bussi[b], Matteo Paloni[a,c,1], and Alessandro Barducci[a,1]

Affiliations are included on p. 6.

Edited by Pablo Debenedetti, Princeton University, Princeton, NJ; received December 3, 2024; accepted March 9, 2025

Biomolecular condensates are currently recognized to play a key role in organizing cellular space and in orchestrating biochemical processes. Despite an increasing interest in characterizing their internal organization at the molecular scale, not much is known about how the densely crowded environment within these condensates affects the structural properties of recruited macromolecules. Here, we adopted explicit-solvent all-atom simulations based on a combination of enhanced sampling approaches to investigate how the conformational ensemble of an RNA hairpin is reshaped in a highly concentrated peptide solution that mimics the interior of a biomolecular condensate. Our simulations indicate that RNA structure is greatly perturbed by this distinctive physico-chemical environment, which weakens RNA secondary structure and promotes extended nonnative conformations. The resulting high-resolution picture reveals that RNA unfolding is driven by the effective solvation of nucleobases through hydrogen bonding and stacking interactions with surrounding peptides. This solvent effect can be modulated by the amino acid composition of the model condensate as proven by the differential RNA behavior observed in the case of arginine-rich and lysine-rich peptides.

RNA folding | membraneless organelles | molecular dynamics | enhanced sampling | protein–RNA interactions

Significance

The complex and crowded cellular environment profoundly influences the structural properties and functions of biomolecules, including RNAs. In particular, biomolecular condensates represent an emerging principle for the compartmentalization of RNA and its regulation. Despite their significance, our understanding of their molecular-scale organization and effects on RNA structure remains limited. In this study, we employ atomistic simulations to investigate RNA properties in a crowded peptide environment resembling biomolecular condensates. Our findings reveal that this environment destabilizes RNA secondary structures and promotes extended nonnative conformations. Notably, the composition of peptides—specifically arginine-rich versus lysine-rich—modulates RNA behavior, suggesting that variations in condensate composition can fine-tune RNA activity in health and disease.

In the cell, RNAs can populate multiple, distinct conformations, and this structural plasticity is intimately connected to their biological activities and tightly regulated by specific processes (1–3).

In this respect, it is particularly intriguing to investigate the potential role of biomolecular condensates, which are currently thought to be crucial players in organizing cellular environment (4). These dynamic nonstoichiometric assemblies are characterized by a high local concentration of specific proteins and nucleic acids and they can act as membrane-less organelles (MLOs) by creating chemically distinct compartments (4–6). The unique physico-chemical environment inside MLOs may significantly reshape the conformational landscape of recruited RNA molecules, potentially providing an effective regulatory mechanism (7).

Recently, a few pioneering studies have explored this hypothesis by probing the RNA properties in model condensates through controlled in vitro experiments (8–12). While experimental evidence suggests that condensate environment can affect the catalytic activity of ribozymes (13, 14), RNA structural characterization in biomolecular condensed phase is limited due to the technical difficulties of most structural biology approaches in nonhomogeneous and/or highly concentrated systems (12, 15). Förster resonance energy transfer (FRET) spectroscopy has provided some insight into the structure of nucleic acids in model MLOs, showing that in vitro condensates can melt duplexes (8, 11) and these findings were recently supported by NMR experiments (16). Regardless of these inspiring results, a clear picture of RNA structural properties in biomolecular condensates, as well as a detailed description of the molecular interactions that likely reshape the conformational ensemble in this environment, are still lacking.

All-atom molecular dynamics (MD) simulations can provide an accurate, high-resolution description of RNA structure and interactions, especially when supplemented with advanced simulation algorithms (17–20). Molecular simulations have also played an important role in the investigation of the dynamical and structural properties of biomolecular condensates. While various coarse-grained models (21–26) are often adopted to effectively tackle the length and time scales associated to these large-sized assemblies, a few studies revealed the potential of all-atom MD simulations in this domain (27–30).

Author contributions: M.P. and A.B. designed research; M.B. performed research; G.B. contributed new reagents/analytic tools; M.B., Y.B., G.B., and M.P. analyzed data; and M.B. and A.B. wrote the paper.

The authors declare no competing interest.

This article is a PNAS Direct Submission.

[1]To whom correspondence may be addressed. Email: m.paloni@ucl.ac.uk or alessandro.barducci@cbs.cnrs.fr.

This article contains supporting information online at https://www.pnas.org/lookup/suppl/doi:10.1073/pnas.2425261122/-/DCSupplemental.

Published April 9, 2025.

In this respect, we recently developed an efficient, fragment-based strategy to shed light on molecular interactions in condensates by performing all-atom MD simulations of high-concentration mixtures of peptides and/or oligonucleotides (31, 32). In this work, we built on these results and we extended this computational approach to investigate the conformational landscape of a small structured RNA in a molecular environment closely mimicking the interior of a biomolecular condensate.

Results

A Minimal System to Investigate RNA Structures in Condensates at the Atomistic Scale. RNA structure is made up of a limited number of secondary and tertiary motifs, which constitute modular units that form complex architectures (33). Among these units, RNA tetraloops, which display a hairpin structure with Watson–Crick base pairing in the stem region and specific noncanonical pairings in a four-base loop, are ubiquitous in large RNAs (34) and hence popular experimental and computational models for investigating RNA structure, dynamics, and folding (35, 36). Here, we chose the GCAA member of the GNRA tetraloop family, whose structure has been solved by NMR and it is characterized by a significant flexibility in the loop region (37, 38).

Inspired by previous results (31, 32), we modeled the physicochemical environment within a biomolecular condensate by simulating the hairpin in a peptide solution with a concentration (around 300 mg/mL) comparable to those observed in model in vitro condensates (28, 39, 40) (Fig. 1*B*). In particular, we selected a polypeptide sequence (RGRGG) based on the RGG/RG motif, which is frequently involved in RNA binding (41) and it is abundant in low-complexity regions of proteins found in MLOs (42). Experimental data suggest that individual RGG/RG motifs bind to RNA weakly but they can establish a dynamical network of multivalent interactions when present in multiple copies and ultimately stabilize protein–RNA condensates (42, 43).

In order to investigate how these intermolecular interactions affect the tetraloop structural properties, we exhaustively sampled its conformational landscape both in the model biomolecular condensed phase and in standard water solution, by combining well-tempered metadynamics (44, 45) and replica exchange with solute tempering (46). The resulting hybrid protocol (WTMetaD-REST2) has been proven to be particularly effective for characterizing the structural ensemble of small RNA molecules (47).

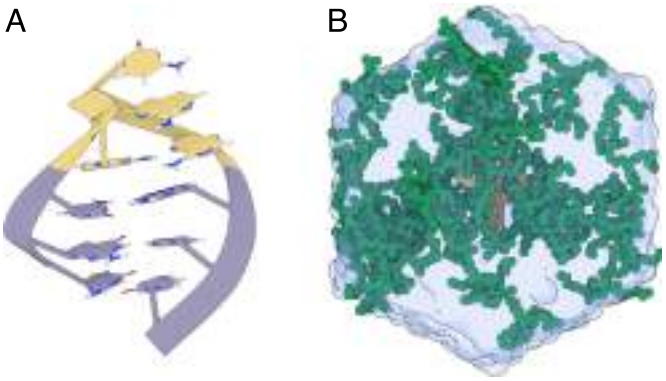

Fig. 1. GCAA tetraloop and biomolecular condensate reconstruction: (*A*) Native structure of GCAA tetraloop (pdb-code: 1ZIH); the stem region is represented in purple, the loop region is in yellow. (*B*) Representative snapshot from the MD simulation of GCAA tetraloop (in yellow) within around 300 mg/mL RGRGG (in green) peptide solution that recreates the chemical environment inside biomolecular condensate.

Extended RNA Conformations Are Favored in Biomolecular Condensed Phase. We report in Fig. 2 the free-energy surfaces (FESs) as a function of structural deviation of the hairpin from the native structure [eRMSD (48)] and its solvent-accessible surface area (SASA) computed using a standard probe radius. In water (Fig. 2*A*) the system exhibits a global free-energy minimum at low values of eRMSD and SASA that corresponds to the native ensemble and encompasses available NMR structures (*SI Appendix*, Fig. S3) (37), whereas a higher-energy basin representing unfolded states is observed at larger values of eRMSD and SASA. This result suggests that the folded hairpin conformation is stable in standard conditions with a predicted folding free-energy $\Delta G_{folding}$ of -14.1 ± 0.2 kJ/mol, in good agreement with experimental $\Delta G_{folding}$ of -12.6 ± 1.0 kJ/mol (49) (*SI Appendix*, Fig. S5). This scenario is dramatically altered in the concentrated peptide solution (Fig. 2*A*). In this environment, the native structure is severely destabilized and the folding landscape is dominated by multiple free-energy minima at higher values of eRMSD. Particularly, the most relevant basin (eRMSD > 1.5, SASA $\sim 26\,nm^2$) corresponds to unfolded states that are more extended than those observed in water solution.

This finding suggests that the model condensate represents a better solvent for the RNA molecule leading to its expansion. In order to dissect the role of the different RNA functional groups in this process, we evaluated the free-energy landscape as a function of the eRMSD and the solvent accessibility of phosphate, base, or sugar groups (Fig. 2*B*). The resulting FESs reveal that in both systems the SASA of phosphate and sugar groups is not particularly affected by the unfolding process whereas the nucleobases are remarkably more solvated in unfolded states. This behavior is particularly pronounced in the biomolecular condensed phase suggesting that the hairpin unfolding in this environment may be attributed to favorable interaction between the RNA bases and the mixed peptide/water solvent.

Destabilization of RNA Secondary Structures in Condensed Phases. Building on this result, we investigated how intermolecular interactions affect RNA base pairing and destabilize the hairpin secondary structure. We first focused on the three canonical Watson–Crick base pairs that define the stem region of the tetraloop (Fig. 3*A*). Remarkably, the free-energies of formation of individual pairs (ΔG) indicate that all these native interactions are considerably stable in water whereas they are disfavored and only transiently observed in the peptide-rich solution. This information can be translated into a more global picture of the folding process by considering the free-energy as a function of the number of native stem base pairs formed for a given conformation (Nc). In agreement with the analysis reported in Fig. 2), the corresponding free-energy profiles (Fig. 3*B*) confirm that the fully formed stem (Nc = 3) is the most stable state in water. Conformations with only two base pairings (Nc = 2) are marginally populated while further loss of base-pairing corresponds to large energy penalties and it ultimately leads to a considerable free-energy difference between the folded and the completely open state (Nc = 0). Conversely, base pairing is significantly destabilized in the model condensate. In this environment, the stem can be described with a heterogeneous structural ensemble, where the folded (Nc = 3) and completely unfolded (Nc = 0) states are similarly populated and separated by higher-energy intermediate states (Fig. 3*B*).

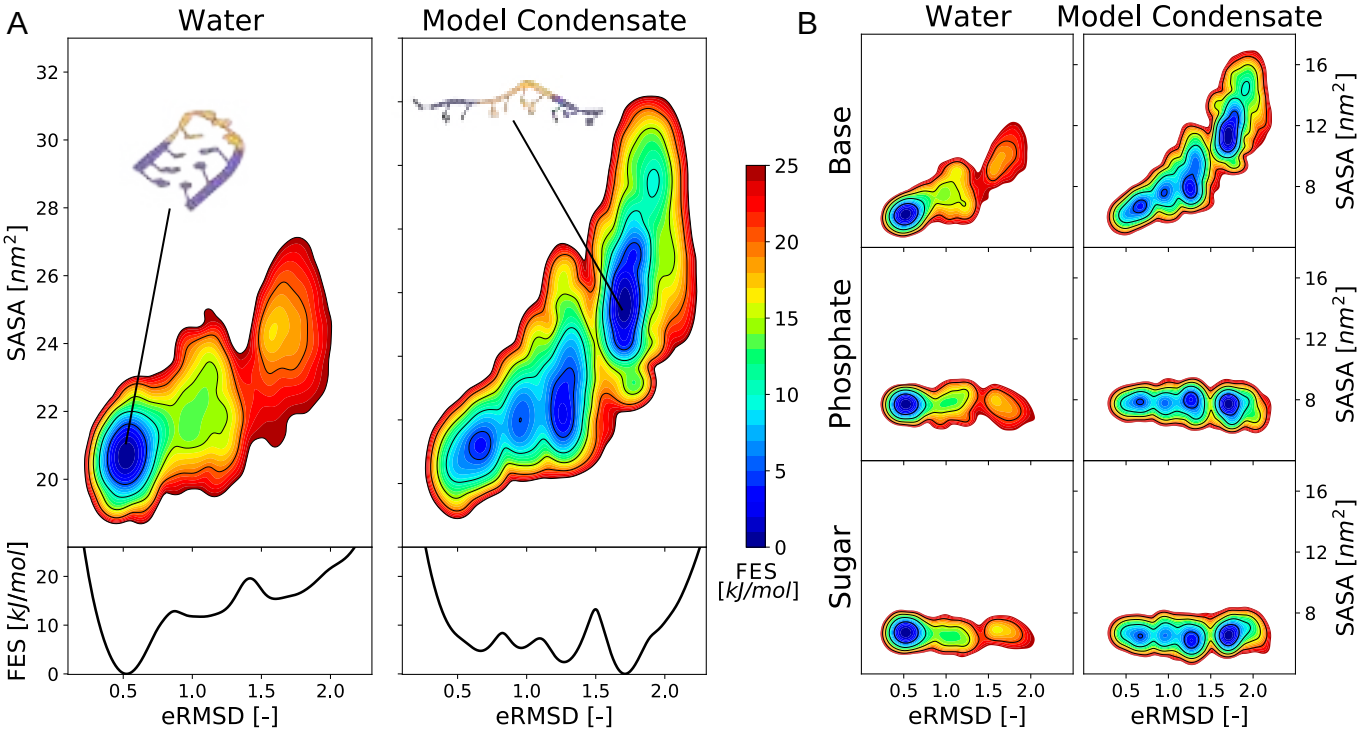

Fig. 2. Extended RNA conformations are favored in biomolecular condensed phase. (*A*) FES as function of eRMSD and SASA, obtained from all-atom MD simulation of GCAA tetraloop in water (*Upper Left*) and in RGRGG peptide solution (300 mg/mL) mimicking the biomolecular condensate environment (*Upper Right*). Molecular representations are reported as an example of GCAA structural conformation corresponding to the main free-energy basin. FES profiles as function of eRMSD for GCAA tetraloop MD simulation in water (*Lower Left*) and in model condensate (*Lower Right*). (*B*) FES as a function of global eRMSD and SASA related to different RNA functional groups: base (*Top*), phosphate (*Center*), and sugar (*Bottom*). The *Left* column is referred to simulation in water while the *Right* one is referred to simulation with model condensate.

Impact of Condensed Phases on RNA Loop Structural Dynamics. Given the major disruption of stable secondary structure in the stem observed in our condensed phase simulations, we then investigated how this environment may affect the structural properties of a flexible region, such as the loop in the GCAA tetraloop (38, 50). To this aim, we limited our analysis to conformations with a fully formed stem (Nc = 3) and we described the structural ensemble of the loop in terms of stacking and pairing interactions among G4–C5–A6–A7 nucleobases.

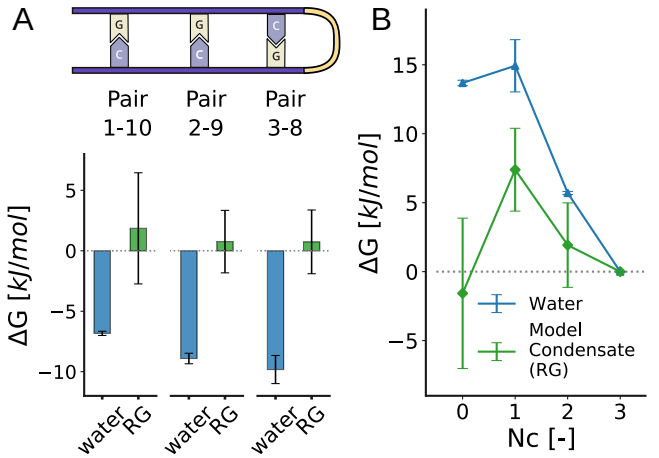

Fig. 3. Destabilization of RNA secondary structures in condensed phases. (*A*) Schematic representation of hairpin stem region (*Top*). Formation free energies (ΔG) of individual pairs (G1–C10, G2–C9, C3–G8, respectively). In blue are the values obtained from the simulation of the RNA in water, in green are the values for the RNA within the model condensate consisting of a solution of RGRGG peptides (indicated RG in the figure) (*Bottom*). (*B*) Free-energy (ΔG) as a function of the number of native stem base pairs formed (*Nc*). *Nc* = 3 indicates the fully formed stem while *Nc* = 0 represents the absence of pairing at the stem level. *Nc* = 1 and *Nc* = 2 correspond to an intermediate condition in which the pairing is partially removed. The blue line indicates RNA in water, and the green line refers to RNA within the model condensate (RG).

Our simulations confirm that the loop is structurally flexible in water and displays a variety of transient interactions, including A6–A7 stacking (∼90% probability), C5–A6 stacking (∼50%), and the G4–A7 noncanonical pairing (70% of which ∼90% trans Sugar–Hoogsteen pairing) (Fig. 4 *A*, *Left*), in very good agreement with NMR-derived conformers (37) (*SI Appendix*, Fig. S3) and with analysis of crystallographic structures (51). This structural ensemble is strongly perturbed in peptide-rich solution where base stacking is significantly weakened and the noncanonical G4–A7 is almost vanished (Fig. 4 *A*, *Right*). Remarkably, the model condensate also induced a characteristic, nonnative G4–A6 pairing (21% of which ∼50% trans Sugar–Hoogsteen), which is never observed in our simulations in water. We note that this alternative pairing has been suggested as a possible folding intermediate in previous MD simulations performed in water (52), although using a different force field.

A more global description of the differential behavior of the loop in the two solvents is provided by the probability maps reported in (Fig. 4*B*), where we summarized the loop conformational ensemble in 12 discrete states associated to specific stacking and pairing patterns. This analysis confirms that, while our simulations correctly capture the loop flexibility suggested by NMR experiments in water (37, 38), they reveal how the condensate environment completely reshapes its conformational ensemble by disfavoring native interactions and possibly promoting nonnative pairing.

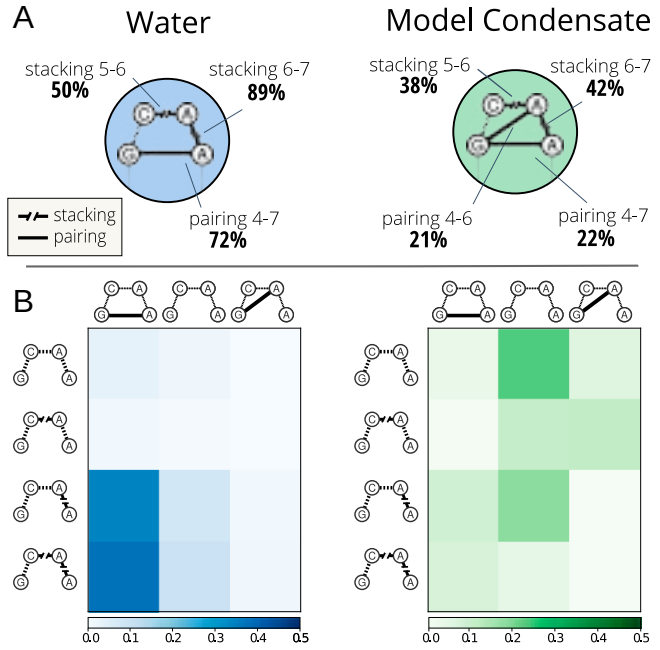

Fig. 4. Impact of condensed phases on RNA loop structural dynamics. (*A*) Diagram of the most relevant structural features in the loop region. Probabilities were obtained by restricting the analysis to hairpin conformations in which the stem is fully formed ($Nc = 3$). On the *Left*, values for RNA in water, on the *Right*, values for RNA inside the model condensate. (*B*) Probability maps of main loop conformational states in terms of pairing and stacking for structures with fully formed stem ($Nc = 3$). In row, states are distinguished in terms of stacking (from top to bottom: no stacking, C5–A6 stacking, A6–A7 stacking, and C5–A6 stacking + A6–A7 stacking); in column, states are distinguished in terms of pairing (from left to right: G4–A7 pairing, no pairing, G4–A6 pairing). In the *Left* panel (blue) the probabilities of RNA in water, in the *Right* (green) the probabilities of RNA inside the condensed model.

Influence of Condensate Composition on RNA Structural Perturbation. Until now we described how our model condensates affect the conformational landscape of GCAA tetraloop, but we have not yet characterized the peptide–RNA interactions that are responsible for the hairpin destabilization. Taking into account the net positive charge of the RGRGG peptide, one can speculate that the electrostatic attraction for the negatively charged RNA hairpin is sufficient to rationalize the observed effects on its structural properties. In order to test this hypothesis and to shed light on the role of the peptide sequence, we then simulated the GCAA tetraloop in a condensed phase of KGKGG peptides, that display the same positive charge but likely differ in terms of molecular interactions with RNA (32). The resulting FES as a function of eRMSD and SASA is reported in Fig. 5, and it shows that while in this condition the GCAA conformational ensemble is significantly reshaped with respect to what observed in water (Fig. 2*A*), the extent of the condensate-induced perturbation is remarkably smaller than in the case of RGRGG peptides (Fig. 2*B*). The comparison of hairpin stability in the diverse environments (Fig. 5 *A*, *Bottom* panel and *SI Appendix*, Fig. S7), further confirms that the lysine-rich model condensate is only mildly destabilizing and it represents an intermediate scenario between water and arginine-rich model condensate. Analysis of SASA (Fig. 5*B*) indicates that while RNA expansion is similar in both model condensates, RGRGG peptides have a larger RNA interaction surface acting as a better RNA solvent. This difference has to be traced back to a stronger propensity of RGRGG peptides to interact with RNA and to induce its unfolding that cannot be rationalized in terms of net electrostatic attraction. We therefore analyzed the H-bonding between peptide side chains and the diverse RNA chemical groups by separately considering the conformations in which the RNA is folded (eRMSD < 1.5) and unfolded (eRMSD > 1.5) (Fig. 5*C*). We first note that overall RGRGG peptides form more H-bonds than KGKGG ones with all chemical groups. Nevertheless, the number of peptide–RNA H-bonds seems not to be affected by RNA (un)folding in most of the cases. Strikingly, the only noticeable exception is observed for arginine-nucleobases H-bonds that significantly increase upon hairpin unfolding. This behavior is not observed in lysine-rich model condensate suggesting a distinctive capability of arginine side chains to strongly interact with unpaired nucleobases, eventually inducing a stronger perturbation on RNA free energy landscape. Furthermore, we expect that this differential destabilization is further reinforced by energetically favorable stacking interactions between nucleobases and arginine guanidinium groups, which preferentially takes place in RNA unfolded states (Fig. 5*D*).

Discussion

Biomolecular condensates have recently emerged as a fundamental organizing principle of the cellular space (4–6). Even if this field of research is still in its infancy and contrasting hypotheses have been proposed about the molecular mechanism of condensate assembly, an increasing body of evidence suggests that biomolecular condensation is a key process for regulating RNA activity inside the cell (53, 54).

Quantitative characterization of this regulation process inherently requires understanding how the peculiar environment of biomolecular condensed phases can affect the conformational ensemble of recruited RNA molecules. In order to shed some light on this topic, we used explicit-solvent all-atom MD simulations to investigate the folding landscape of an RNA tetraloop in a highly concentrated solution of an arginine-rich peptide, which mimics the interior of a biomolecular condensate.

To this aim, we relied on an efficient enhanced sampling method based on the combination of WT-MetaD (44, 45) and replica-exchange solute tempering method (REST2) (46) that has been successfully applied to determine the conformational landscape of several RNA hairpins in standard conditions (47). Similarly, we first took advantage of this computational strategy to predict a folding free-energy landscape of the GCAA tetraloop in water solution. Our results are in good agreement with previous MD simulations (20, 36) performed using a very similar force field but different enhanced sampling methods, confirming the effectiveness of REST2-MetaD protocol. Importantly, our results are also in good agreement with available NMR structures (37) and thermodynamic data from calorimetry experiments (49, 55), thus confirming the accuracy of last-generation RNA force fields (56) for this class of systems.

Most importantly, we then employed this advanced simulation scheme to determine the free-energy landscape of the system in our model biomolecular condensed phase, thus providing remarkable picture of RNA conformational ensemble in these extreme conditions. Our simulations revealed that the condensate environment completely reshapes the FES of the GCAA tetraloop leading to a rugged surface (Fig. 1) with multiple basins, where the native structure does no longer represent the global free-energy minimum. The resulting heterogeneous landscape is in good agreement with FRET experiments suggesting a significant structural disorder and a rich conformational dynamics for small single-stranded RNA molecules in LAF-1 condensates

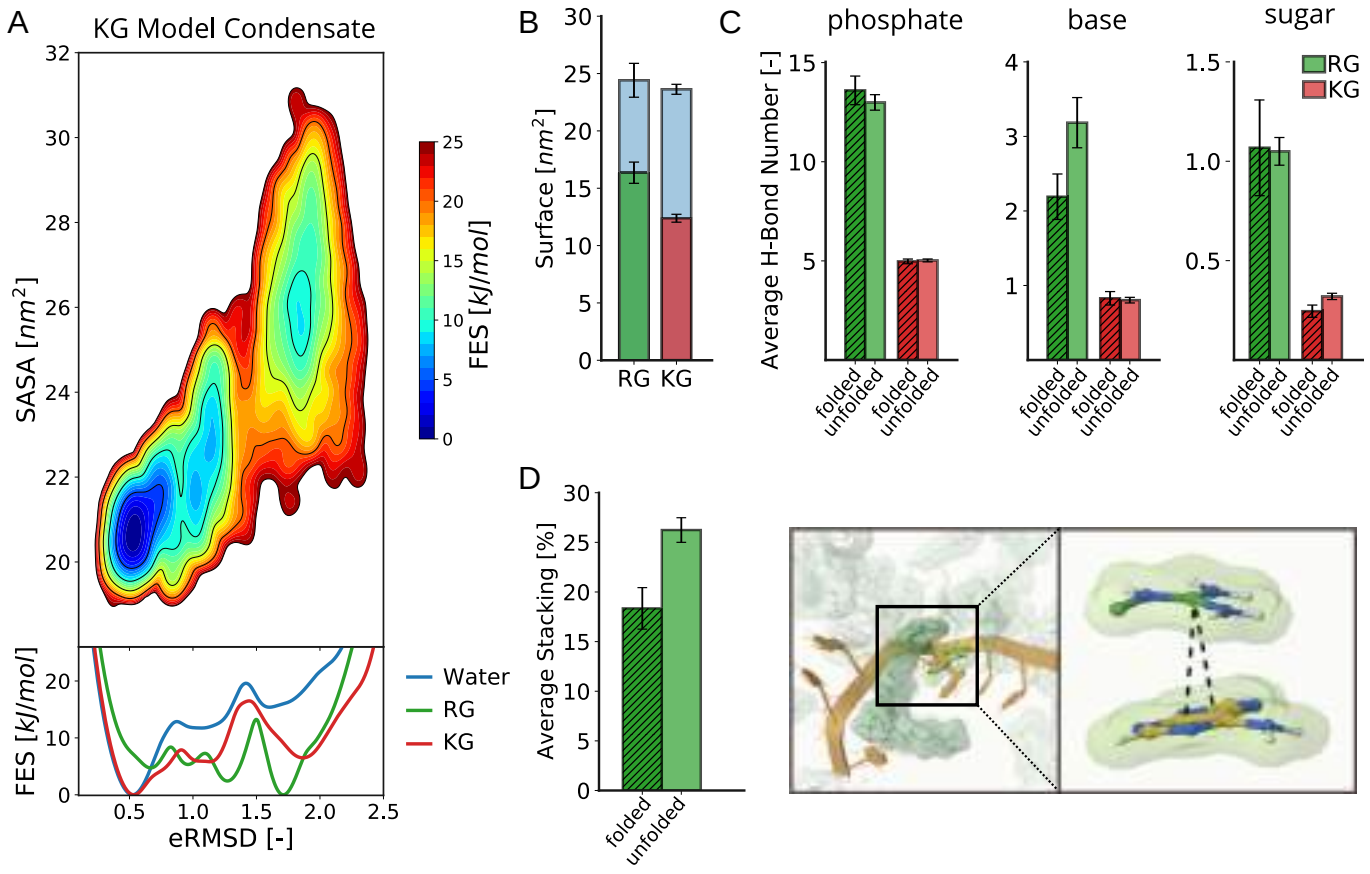

Fig. 5. Influence of condensate composition on RNA structural perturbation. (*A*) FES as function of eRMSD and SASA, obtained from simulation of GCAA tetraloop in KGKGG peptide solution (KG model condensate) (*Top*). FES profiles as function of eRMSD for GCAA tetraloop simulation in water (blue), RG model condensate (green), and KG model condensate (red) (*Bottom*). (*B*) In blue are reported tetraloop SASA in RG model condensate (*Left*) and in KG model condensate (*Right*). In green is represented the RNA–peptides interaction surface in RG model condensate (*Left*) while in red the RNA–peptides interaction surface in KG model condensate (*Right*). (*C*) Average hydrogen bond number between RNA and peptide side chains, reported for different RNA functional groups: phosphate (*Left*), base (*Center*), and sugar (*Right*). Hatched bars are referred to folded hairpin conformations ($eRMSD < 1.5$) while unhatched bars are referred to unfolded conformations ($eRMSD > 1.5$). In green RG model condensate while in red KG model condensate. (*D*) Average percentage of hairpin nucleobases forming intermolecular stacking interactions with the arginine guanidinium group in RG model condensate. The hatched bar is referred to folded hairpin conformations ($eRMSD < 1.5$) while unhatched bar is referred to unfolded conformations ($eRMSD > 1.5$). On the right is a molecular representation of intermolecular stacking interaction between GCAA nucleobase and guanidinium group.

(57, 58). Furthermore, our simulations indicate that direct interactions between the peptides and the RNA bases greatly destabilize the RNA secondary structure and ultimately favor open, unfolded conformations. This destabilization of RNA base pairing is compatible with multiple experimental findings, such as the melting of nucleic acid duplexes in model condensate of disordered N-terminus of DDX4 proteins (8) or the disruption of the s2m RNA stem-loop structure within a condensate of the SARS-CoV-2 nucleocapsid protein (59). Beyond the overall destabilization, our simulations reveal the partial stabilization of alternative, nonnative base pairing in the flexible loop of the GCAA hairpin. While the extent of this phenomenon is limited in the model system investigated here, this finding supports the fascinating hypothesis that cellular condensates may induce alternative functionally relevant structural arrangements in larger RNA molecules. Even if present computational resources do not allow to characterize the structural ensemble of complex cellular RNAs by atomistic MD, the development of CG models for RNA in condensates (24, 60) may provide a complementary approach to tackle this challenge.

Overall, the structural perturbation and conformational redistribution effects are likely tuned by the chemical composition of the condensate. In order to shed more light on this topic, we tested the hairpin behavior in a similar yet distinct environment by substituting arginine with lysine residues in the peptide sequence. The resulting FES indicates that lysine-rich peptides are less destabilizing and lead to a smaller perturbation of the RNA conformational ensemble, in agreement with the experimental observation that polyR/polyD coacervates dissolve RNA duplexes whereas this "helicase activity" is less evident for polyK/polyD condensates (11). In this respect, our results indicate that arginine side chains interact more effectively with RNA than lysine. In particular, the guanidinium groups can establish a higher number of hydrogen bonds with phosphate, sugar, and nucleobases. In the context of RNA conformational dynamics, arginine–base interactions are particularly relevant since they significantly increase upon RNA unfolding and remarkably stabilizing extended conformations, at variance with what is observed for lysine. This differential destabilizing behavior is further reinforced by arginine propensity of forming stacking interactions with RNA bases with a mechanism reminiscent of what has been proposed to rationalize urea-driven denaturation of structured RNAs (61).

Overall, our work shows that biomolecular condensates may play a central role in regulating the biological activity of RNA within the cell by altering their conformational ensemble. In

condensed phase, the dynamic network of intermolecular interactions can significantly perturb conformational distribution and affect energy barriers possibly favoring conformational excited states with functional relevance. Moreover, dysregulation of RNA structural ensembles has been linked to various human diseases (62–64). In this context, elucidating the regulatory role of biomolecular condensates in RNA conformational dynamics could provide insight into the molecular basis of these conditions and reveal potential therapeutic targets for RNA-associated pathologies.

Materials and Methods

MD simulations were performed using GROMACS 2021.4 (65) patched with PLUMED 2.8 (66, 67) to perform Well-Tempered Metadynamics (44) (WT-MetaD) and using a general Hamiltonian replica exchange implementation (68). The initial conformation of the (GGCGCAAGCC) RNA tetraloop was the model 1 of NMR structures deposited as Protein Data Bank (PDB) entry from 1ZIH pdb (37). The GCAA tetraloop was modeled with the DES-Amber force field developed by Shaw and coworkers (56). In the REST2 (46) framework, 16 replicas were simulated in the effective temperature range 300 to 700 K (using scaling factors in a geometric series ranging from 1.0 to 0.414). As collective variables biased for WT-MetaD (44) were used in combination eRMSD metric (48) and the gyration radius calculated over all the heavy atoms of RNA backbone (R_{gyr}^{bb}). Further details about the simulation protocol and analysis methods are available in *SI Appendix*.

Data, Materials, and Software Availability. Molecular dynamics trajectories data have been deposited in Zenodo (https://doi.org/10.5281/zenodo.14203857) (69).

ACKNOWLEDGMENTS. We acknowledge the support of the Swiss National Science Foundation under Grant CRSII5_193740 and of the French Agence Nationale de la Recherche under grant ANR-21-CE30-0001 and ANR-21-CE11-0037. M.B. was supported by funds of the LabMuse EpiGenMed. G.B. acknowledges the Italian National Centre for High Performance Computing, Big Data, and Quantum Computing (Grant No. CN00000013), funded within the Next Generation European Union initiative. This work was granted access to the HPC resources of Centre Informatique National de l'Enseignement Superieur under the allocation 2021-A0100712465 made by Grand Equipement National de Calcul Intensif.

Author affiliations: [a]Centre de Biologie Structurale, Université de Montpellier, CNRS, INSERM, Montpellier 34090, France; [b]Molecular and Statistical Biophysics, Scuola Internazionale Superiore di Studi Avanzati, Trieste 34136, Italy; and [c]Department of Chemical Engineering, Thomas Young Centre, University College London, London WC1E 7JE, United Kingdom

1. M. L. Ken *et al.*, RNA conformational propensities determine cellular activity. *Nature* **617**, 835–841 (2023).
2. J. A. Cruz, E. Westhof, The dynamic landscapes of RNA architecture. *Cell* **136**, 604–609 (2009).
3. A. M. Mustoe, C. L. Brooks, H. M. Al-Hashimi, Hierarchy of RNA functional dynamics. *Annu. Rev. Biochem.* **83**, 441–466 (2014).
4. S. F. Banani, H. O. Lee, A. A. Hyman, M. K. Rosen, Biomolecular condensates: Organizers of cellular biochemistry. *Nat. Rev. Mol. Cell Biol.* **18**, 285–298 (2017).
5. A. A. Hyman, C. A. Weber, F. Jülicher, Liquid–liquid phase separation in biology. *Annu. Rev. Cell Dev. Biol.* **30**, 39–58 (2014).
6. Y. Shin, C. P. Brangwynne, Liquid phase condensation in cell physiology and disease. *Science* **357**, eaaf4382 (2017).
7. L. R. Ganser, M. L. Kelly, D. Herschlag, H. M. Al-Hashimi, The roles of structural dynamics in the cellular functions of RNAs. *Nat. Rev. Mol. Cell Biol.* **20**, 474–489 (2019).
8. T. J. Nott, T. D. Craggs, A. J. Baldwin, Membraneless organelles can melt nucleic acid duplexes and act as biomolecular filters. *Nat. Chem.* **8**, 569–575 (2016).
9. E. M. Langdon *et al.*, mRNA structure determines specificity of a polyQ-driven phase separation. *Science* **360**, 922–927 (2018).
10. F. P. Cakmak, S. Choi, M. O. Meyer, P. C. Bevilacqua, C. D. Keating, Prebiotically-relevant low polyion multivalency can improve functionality of membraneless compartments. *Nat. Commun.* **11**, 5949 (2020).
11. S. Choi, M. O. Meyer, P. C. Bevilacqua, C. D. Keating, Phase-specific RNA accumulation and duplex thermodynamics in multiphase coacervate models for membraneless organelles. *Nat. Chem.* **14**, 1110–1117 (2022).
12. M. O. Meyer, R. Yamagami, S. Choi, C. D. Keating, P. C. Bevilacqua, RNA folding studies inside peptide-rich droplets reveal roles of modified nucleosides at the origin of life. *Sci. Adv.* **9**, eadh5152 (2023).
13. R. R. Poudyal *et al.*, Template-directed RNA polymerization and enhanced ribozyme catalysis inside membraneless compartments formed by coacervates. *Nat. Commun.* **10**, 490 (2019).
14. J. M. Iglesias-Artola *et al.*, Charge-density reduction promotes ribozyme activity in RNA-peptide coacervates via RNA fluidization and magnesium partitioning. *Nat. Chem.* **14**, 407–416 (2022).
15. I. Peran, T. Mittag, Molecular structure in biomolecular condensates. *Curr. Opin. Struct. Biol.* **60**, 17–26 (2020).
16. A. K. Rangadurai *et al.*, Phase separation modulates the thermodynamics and kinetics of RNA hybridization. *J. Am. Chem. Soc.* **146**, 19686–19689 (2024).
17. S. Bottaro, P. Banas, J. Sponer, G. Bussi, Free energy landscape of GAGA and UUCG RNA tetraloops. *J. Phys. Chem. Lett.* **7**, 4032–4038 (2016).
18. J. Sponer *et al.*, RNA structural dynamics as captured by molecular simulations: A comprehensive overview. *Chem. Rev.* **118**, 4177–4338 (2018).
19. V. Mlỳnskỳ, G. Bussi, Exploring RNA structure and dynamics through enhanced sampling simulations. *Curr. Opin. Struct. Biol.* **49**, 63–71 (2018).
20. G. H. Zerze, P. M. Piaggi, P. G. Debenedetti, A computational study of RNA tetraloop thermodynamics, including misfolded states. *J. Phys. Chem. B* **125**, 13685–13695 (2021).
21. G. L. Dignon, W. Zheng, Y. C. Kim, R. B. Best, J. Mittal, Sequence determinants of protein phase behavior from a coarse-grained model. *PLoS Comput. Biol.* **14**, e1005941 (2018).
22. J. M. Choi, F. Dar, R. V. Pappu, LASSI: A lattice model for simulating phase transitions of multivalent proteins. *PLoS Comput. Biol.* **15**, e1007028 (2019).
23. Z. Benayad, S. von Bulow, L. S. Stelzl, G. Hummer, Simulation of FUS protein condensates with an adapted coarse-grained model. *J. Chem. Theory Comput.* **17**, 525–537 (2020).
24. H. T. Nguyen, N. Hori, D. Thirumalai, Condensates in RNA repeat sequences are heterogeneously organized and exhibit reptation dynamics. *Nat. Chem.* **14**, 775–785 (2022).
25. J. A. Joseph *et al.*, Physics-driven coarse-grained model for biomolecular phase separation with near-quantitative accuracy. *Nat. Comput. Sci.* **1**, 732–743 (2021).
26. G. Tesei, K. Lindorff-Larsen, Improved predictions of phase behaviour of intrinsically disordered proteins by tuning the interaction range. *Open Res. Eur.* **2**, 94 (2022).
27. W. Zheng *et al.*, Molecular details of protein condensates probed by microsecond long atomistic simulations. *J. Phys. Chem. B* **124**, 11671–11679 (2020).
28. N. Galvanetto *et al.*, Extreme dynamics in a biomolecular condensate. *Nature* **619**, 876–883 (2023).
29. A. A. Polyansky, L. D. Gallego, R. G. Efremov, A. Köhler, B. Zagrovic, Protein compactness and interaction valency define the architecture of a biomolecular condensate across scales. *eLife* **12**, e80038 (2023).
30. S. Mukherjee, L. V. Schäfer, Thermodynamic forces from protein and water govern condensate formation of an intrinsically disordered protein domain. *Nat. Commun.* **14**, 5892 (2023).
31. M. Paloni, R. Bailly, L. Ciandrini, A. Barducci, Unraveling molecular interactions in liquid–liquid phase separation of disordered proteins by atomistic simulations. *J. Phys. Chem. B* **124**, 9009–9016 (2020).
32. M. Paloni, G. Bussi, A. Barducci, Arginine multivalency stabilizes protein/RNA condensates. *Protein Sci.* **30**, 1418–1426 (2021).
33. I. Tinoco Jr, C. Bustamante, How RNA folds. *J. Mol. Biol.* **293**, 271–281 (1999).
34. C. Woese, S. Winker, R. Gutell, Architecture of ribosomal RNA: Constraints on the sequence of "tetra-loops". *Proc. Natl. Acad. Sci. U.S.A.* **87**, 8467–8471 (1990).
35. S. Nozinovic, B. Fürtig, H. R. Jonker, C. Richter, H. Schwalbe, High-resolution NMR structure of an RNA model system: The 14-mer cUUCGg tetraloop hairpin RNA. *Nucleic Acids Res.* **38**, 683–694 (2010).
36. D. Tan, S. Piana, R. M. Dirks, D. E. Shaw, RNA force field with accuracy comparable to state-of-the-art protein force fields. *Proc. Natl. Acad. Sci. U.S.A.* **115**, E1346–E1355 (2018).
37. F. M. Jucker, H. A. Heus, P. F. Yip, E. H. Moors, A. Pardi, A network of heterogeneous hydrogen bonds in GNRA tetraloops. *J. Mol. Biol.* **264**, 968–980 (1996).
38. L. Zhao, T. Xia, Direct revelation of multiple conformations in RNA by femtosecond dynamics. *J. Am. Chem. Soc.* **129**, 4118–4119 (2007).
39. J. P. Brady *et al.*, Structural and hydrodynamic properties of an intrinsically disordered region of a germ cell-specific protein on phase separation. *Proc. Natl. Acad. Sci. U.S.A.* **114**, E8194–E8203 (2017).
40. A. C. Murthy *et al.*, Molecular interactions underlying liquid–liquid phase separation of the FUS low-complexity domain. *Nat. Struct. Mol. Biol.* **26**, 637–648 (2019).
41. P. Thandapani, T. R. O'Connor, T. L. Bailey, S. Richard, Defining the RGG/RG motif. *Mol. Cell* **50**, 613–623 (2013).
42. P. A. Chong, R. M. Vernon, J. D. Forman-Kay, RGG/RG motif regions in RNA binding and phase separation. *J. Mol. Biol.* **430**, 4650–4665 (2018).
43. K. Takahama, K. Kino, S. Arai, R. Kurokawa, T. Oyoshi, Identification of Ewing's sarcoma protein as a G-quadruplex DNA- and RNA-binding protein. *FEBS J.* **278**, 988–998 (2011).
44. A. Barducci, G. Bussi, M. Parrinello, Well-tempered metadynamics: A smoothly converging and tunable free-energy method. *Phys. Rev. Lett.* **100**, 020603 (2008).
45. A. Laio, M. Parrinello, Escaping free-energy minima. *Proc. Natl. Acad. Sci. U.S.A.* **99**, 12562–12566 (2002).
46. L. Wang, R. A. Friesner, B. Berne, Replica exchange with solute scaling: A more efficient version of replica exchange with solute tempering (REST2). *J. Phys. Chem. B* **115**, 9431–9438 (2011).
47. V. Mlynsky *et al.*, Toward convergence in folding simulations of RNA tetraloops: Comparison of enhanced sampling techniques and effects of force field modifications. *J. Chem. Theory Comput.* **18**, 2642–2656 (2022).
48. S. Bottaro, F. Di Palma, G. Bussi, The role of nucleobase interactions in RNA structure and dynamics. *Nucleic Acids Res.* **42**, 13306–13314 (2014).
49. J. SantaLucia Jr, R. Kierzek, D. H. Turner, Context dependence of hydrogen bond free energy revealed by substitutions in an RNA hairpin. *Science* **256**, 217–219 (1992).
50. L. Trantírek, E. Caha, P. Kadeřávek, R. Fiala, NMR 13C-relaxation study of base and sugar dynamics in GCAA RNA hairpin tetraloop. *J. Biomol. Struct. Dyn.* **25**, 243–252 (2007).

51. S. Bottaro, A. Gil-Ley, G. Bussi, RNA folding pathways in stop motion. *Nucleic Acids Res.* **44**, 5883–5891 (2016).
52. R. G. Viegas *et al*., Characterizing the folding transition-state ensembles in the energy landscape of an RNA tetraloop. *J. Chem. Inf. Model.* **63**, 5641–5649 (2023).
53. H. J. Wiedner, J. Giudice, It's not just a phase: Function and characteristics of RNA-binding proteins in phase separation. *Nat. Struct. Mol. Biol.* **28**, 465–473 (2021).
54. N. Ripin, R. Parker, Formation, function, and pathology of RNP granules. *Cell* **186**, 4737–4756 (2023).
55. T. Dale, R. Smith, M. J. Serra, A test of the model to predict unusually stable RNA hairpin loop stability. *RNA* **6**, 608–615 (2000).
56. M. R. Tucker, S. Piana, D. Tan, M. V. LeVine, D. E. Shaw, Development of force field parameters for the simulation of single-and double-stranded DNA molecules and DNA–protein complexes. *J. Phys. Chem. B* **126**, 4442–4457 (2022).
57. S. Elbaum-Garfinkle *et al*., The disordered p granule protein LAF-1 drives phase separation into droplets with tunable viscosity and dynamics. *Proc. Natl. Acad. Sci. U.S.A.* **112**, 7189–7194 (2015).
58. Y. Kim, S. Myong, RNA remodeling activity of dead box proteins tuned by protein concentration, RNA length, and ATP. *Mol. Cell* **63**, 865–876 (2016).
59. T. de Vries *et al*., Specific protein–RNA interactions are mostly preserved in biomolecular condensates. *Sci. Adv.* **10**, eadm7435 (2024).
60. I. Yasuda *et al*., Coarse-grained model of disordered RNA for simulations of biomolecular condensates. *J. Chem. Theory Comput.* **21**, 2766–2779 (2025).
61. U. D. Priyakumar, C. Hyeon, D. Thirumalai, A. D. MacKerell Jr, Urea destabilizes RNA by forming stacking interactions and multiple hydrogen bonds with nucleic acid bases. *J. Am. Chem. Soc.* **131**, 17759–17761 (2009).
62. V. Bernat, M. D. Disney, RNA structures as mediators of neurological diseases and as drug targets. *Neuron* **87**, 28–46 (2015).
63. B. A. Conti, M. Oppikofer, Biomolecular condensates: New opportunities for drug discovery and RNA therapeutics. *Trends Pharmacol. Sci.* **43**, 820–837 (2022).
64. R. Bose, I. Saleem, A. M. Mustoe, Causes, functions, and therapeutic possibilities of RNA secondary structure ensembles and alternative states. *Cell Chem. Biol.* **31**, 17–35 (2024).
65. M. J. Abraham *et al*., GROMACS: High performance molecular simulations through multi-level parallelism from laptops to supercomputers. *SoftwareX* **1**, 19–25 (2015).
66. G. A. Tribello, M. Bonomi, D. Branduardi, C. Camilloni, G. Bussi, PLUMED 2: New feathers for an old bird. *Comput. Phys. Commun.* **185**, 604–613 (2014).
67. TP Consortium, Promoting transparency and reproducibility in enhanced molecular simulations. *Nat. Methods* **16**, 670–673 (2019).
68. G. Bussi, Hamiltonian replica exchange in GROMACS: A flexible implementation. *Mol. Phys.* **112**, 379–384 (2014).
69. M. Boccalini *et al*., Research data supporting: "Exploring RNA destabilization mechanisms in biomolecular condensates through atomistic Simulations". Zenodo. https://doi.org/10.5281/zenodo.14203857. Deposited 19 September 2024.